The effect of organoclay addition on the properties of an acrylate based, thermally activated shape memory polymer

BARWOOD, Michael J., BREEN, Christopher <http://orcid.org/0000-0002-5637-9182>, CLEGG, Francis <http://orcid.org/0000-0002-9566-5739> and HAMMOND, Carol L.

The effect of organoclay addition on the properties of an acrylate based, thermally activated shape memory polymer.

Michael J. Barwood[a,1], Chris Breen[a,*], Francis Clegg[a], Carol L. Hammond[b]

[a]*Materials and Engineering Research Institute, Sheffield Hallam University, Sheffield, S1 1WB, UK*
[b] *Multipackaging Solutions, Millenium Way West, Phoenix Centre, Nottingham, NG6 6AW, UK*

ABSTRACT

Shape Memory Polymers (~~SMP~~SMPs) exhibit the intriguing ability to change back from an intermediate, deformed shape back to their original, permanent shape. In this contribution a systematic series of t-butylacrylate-*co*-poly(ethyleneglycol) dimethacrylate (tBA-*co*-PEGDMA) polymers have been synthesised and characterised prior to incorporation of organoclay. Increasing the poly(ethyleneglycol) dimethacrylate (PEGDMA) content in increments of 10% increased the storage modulus from 2005 to 2250 MPa, reduced the glass transition temperature from +41 to -26^{o}C and reduced the intensity of the associated tan δ peak. The tBA-*co*-PEGDMA crosslinked networks displayed useful shape memory properties up to PEGDMA contents of 40 %. Above this PEGDMA percentage the materials were prone to fracture and too brittle for a realistic assessment of their shape memory capability. The system containing 90% t-butylacrylate (tBA) and 10% PEGDMA was selected as the host matrix to investigate how the incorporation of 1 to 5 mass% of a benzyl tallow dimethylammonium-exchanged bentonite, (BTDB) influenced the shape memory properties. X-ray diffraction data confirmed that BTDB formed a microcomposite in the selected matrix and exerted no influence on the storage modulus, rubbery modulus, glass transition temperature, T_g, or the shape or intensity of the tan δ peak of the host matrix. Therefore, it was anticipated that the presence of BTDB would have no effect, positive or negative, nor on the shape memory properties of the host matrix. However, it was found that the incorporation of clay, especially at the 1 mass% level, significantly accelerated the speed, compared ~~to~~ with the clay-free ~~SMP~~SMPs, at which the microcomposite returned to the original, permanent shape. This accelerated return to the permanent shape was also observed when the microcomposite was coated onto a 100 µm PET film.

Keywords
Shape memory polymer, nanocomposite, organoclay, polyacrylate

Corresponding Author:
Professor Chris Breen, Materials and Engineering Research Institute, Sheffield Hallam University, Sheffield S1 1WB, UK. Phone +44-1142253008. E-mail: c.breen@shu.ac.uk
Contact details for other authors:
Dr. Francis Clegg, Materials and Engineering Research Institute, Sheffield Hallam University, Sheffield S1 1WB, UK. Phone +44-1142253062. E-mail: f.clegg@shu.ac.uk
Dr. Michael Barwood, Materials and Engineering Research Institute, Sheffield Hallam University, Sheffield S1 1WB, UK. Phone +44-1142253008. E-mail: m.barwood@lboro.ac.uk
Carol Hammond, Multipackaging Solutions, Millenium Way West, Phoenix Centre, Nottingham, NG6 6AW, UK. carol.hammond@multipkg.com

[1] Dr. Michael Barwood, Centre for Sustainable Manufacturing and Recycling Technologies, Wolson School of Mechnical and Manufacturing Engineering, Loughborough University, Leicestershire, LE11 3TU, UK.

1. Introduction.

Shape memory polymers (~~SMP~~SMPs) have the ability to store a permanent shape and be deformed into a temporary shape by applying an external stress and temperature. This temporary shape is stored by cooling into the dormant shape, in which it remains, until it is encouraged to return to its original, permanent shape (~~Figure~~Fig. 1). The transformation from the stressed temporary shape back to the permanent, stress-free shape is usually triggered by thermal (Liff et al., 2007), electrical (Liu et al., 2009), or other environmental stimuli e.g. UV or visible radiation (Jiang et al., 2006). This change from temporary to permanent shape is essentially driven by the elastic strain stored in the dormant shape during the initial deformation into the temporary shape (Liu et al., 2007).

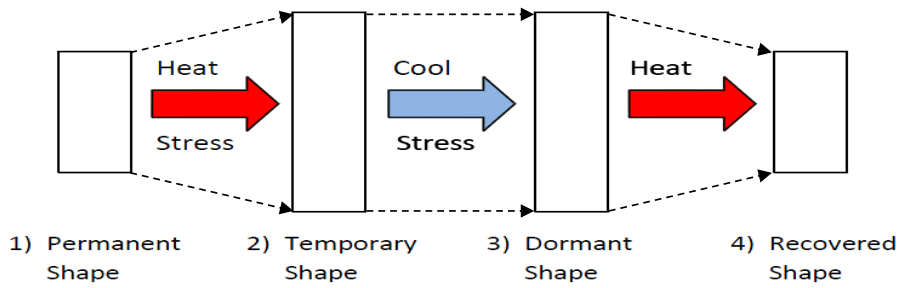

Fig. 1. Schematic depiction of the unconstrained shape memory effect (SME) of a thermally activated SMP.

The most common ~~SMP~~SMPs are thermally-responsive, which means that the material is deformed into its temporary shape, at one temperature and a second thermal change is required to initiate the return to its original, permanent, shape. The temperature at which this change in shape occurs is referred to as the transition temperature, T_{trans}, and is typically the glass transition temperature, T_g, or melting transition temperature, T_m, of the polymer. The unique, 'tunable' properties of ~~SMP~~SMPs make them attractive for a number of potential applications in almost every avenue of life, ranging from self-repairing car bodies (Ikematu et

al., 1993), kitchen utensils (Lendlein and Kelch, 2002), switches to sensors (Liu et al., 2009), intelligent packaging (Behl et al., 2010), toys (Ikematu et al., 1993) and tools (Tong, 2004). A significant number of studies have focussed on the use of ~~SMP~~SMPs in biomedical applications including sutures (Lendlein and Langer, 2002), stents (Venkatraman et al., 2006), catheters (Liu et al., (2007), micro-actuators (Maitland et al., 2002) and tissue scaffolds (Migneco et al., 2009). More recently, the focus has moved towards ~~SMP~~SMPs with two temporary shapes which transform in response to two different stimulus events (Behl et al., 2010; Tao, 2010; Ge et al., 2013).

Two commonly adopted approaches to improve and expand the applications of ~~SMP~~SMPs are 1) optimise the polymer system's mechanical, thermal and shape memory properties for the intended application and/or, 2) incorporate nanomaterials into the optimised polymer to provide additional property enhancements. The knowledge that the incorporation of 1 to 5 mass% of well dispersed clay can increase both the tensile properties and the storage modulus of the host polymer (Annabi-Bergaya, 2008; Utracki, 2010) means that a clay polymer nanocomposite (CPN) has the potential to increase the energy stored within the temporary shape of a SMP; giving it the ability to exert a stronger physical force when returning to the original shape and/or transform at a faster rate. Despite their potential to improve shape memory properties, clays have not been extensively studied. Most reports focus on their positive influence on polyurethanes (PU) at organoclay (OC) levels of 0.5 to 2 mass% (Cao and Jana, 2007; Chung et al., 2011; Haghayegh and Sadeghi, 2012) although larger quantities of calcined attapulgite (Xu et al., 2009) and grafted bentonite (Wu et al., 2013) were required. Rezanejad and Kokabi (2007) established that adding 12 mass% of Cloisite 15A (a dihydrogenated tallow dimethyl ammonium-bentonite) increased the recovery stress by 200%. Finally, OC have been used to improve the shape memory properties of epoxy CPN (Liu et al., 2011) and nanofoams (Quadrini et al., 2012).

Acrylate polymers represent an ideal system for SMP/clay studies since the copolymerization of linear acrylates (mono-functional monomers) with acrylate cross linkers (multifunctional monomers) yields ~~SMP~~SMPs with tuneable properties that can be optimi~~s~~z~~z~~ed for specific applications (Safranski and Gall, 2008; Voit et al., 2010). Previous investigations by Yang et al., (2007), Yakacki et al., (2008) and Ortega et al., (2008) have shown that tert-butylacrylate-*co*-poly(ethylene glycol) dimethacrylate (tBA-*co*-PEGDMA) networks have shape memory ability with thermal and mechanical properties that can be readily tailored. In this particular example a transition temperature near 40 °C was required.

To our knowledge the enhancement of tBA-*co*-PEGDMA networks via incorporation of OC has yet to be reported, thus this contribution represents a benchmark study designed to explore the impact of clay on the properties of an optimised acrylate based SMP system. It aims to identify the influence of the OC loading on a UV polymerised polyacrylate system, of selected stoichiometry, and the effect on the resulting physical properties. The features under investigation are; the OC loading required to influence the shape memory effect of self-supporting polymer films (and when coated onto a PET substrate); the effect of OC loading on the storage moduli, the glass transition temperature, and, in particular, macroscopic effects including the shape fixity, the extent of shape recovery as well as the time required to return to the original, permanent shape.

2. Experimental

2.1 Materials

The mono-functional acrylate tert-butyl acrylate (tBA), the di-functional acrylate poly(ethylene glycol) dimethacrylate (PEGDMA), with an average molecular weight of 750 g mol^{-1}, the photoinitiator 2,2-dimethoxy-2-phenylacetophenone (DMPA) and accelerator ethyl-4-(dimethylamino) benzoate (EDB) were purchased from Sigma-Aldrich and used as

119 received. The purity of tBA was 98%, while the purities of the other reagents were ≥ 99%.
120 The Cloisite 10A (C10A), is a bentonite in which the resident Na^+-cations have been replaced
121 by quaternary benzyl hydrogenatedtallow dimethylammonium ions, and was supplied by
122 Rockwood Specialties Inc., UK. The substrate material used in the coating studies was a 100
123 μm thick polyethylene terephthalate (PET) film (HiFi Films Ltd.).

124 *2.2 Pre-treatment of commercial organoclay*
125 Initial attempts to fully polymerise the tBA-*co*-PEGDMA systems in the presence of as-
126 received C10A were unsuccessful and the excess surfactant present on C10A was identified
127 as the cause. The excess organomodifier was removed, prior to use, by dispersion in water
128 whilst stirring at 80 °C for 1 h, then filtered and washed with propan-2-ol. This was repeated
129 6 times before drying at 70°C for 4 h. The fully washed material is subsequently referred to
130 as benzyl tallow dimethylammonium-bentonite (BTDB).

131 *2.3 Preparation of polymers and PCN*

132 *2.3.1 tBA-co-PEGDMA*
133 A series of polymer networks were prepared using selected ratios of the monomers (Table 1).
134 The tBA, PEGDMA, DMPA and EDB were weighed out and added together in a glass vial,
135 wrapped in foil and the solution was magnetically stirred for 30 mins at ca. 22°C. The
136 solution was then sonicated for an additional 30 mins before photopolymerisation (see
137 Section 2.3.3 below).

138 *2.3.2 tBA-co-PEGDMA/BTBD*
139 The tBA90/PEGDMA10 polymer network was used as a host matrix for selected quantities
140 of BTBD (Table 1). The procedure was similar to that described above except that the
141 mixture was stirred for 24 h at ca. 22°C, before sonication and photopolymerisation (Decker
142 et al., 2005).

143 *2.3.3 Polymer Photopolymerisation*

144 Photopolymerisation of stirred and ultrasonicated mixtures was carried out in a mould
145 constructed using two ultraviolet (UV) clear glass slides, 100 x 100 x 1 mm^3, to which UV
146 clear PET film liners, 12 x 12 x 0.1 mm^3 were attached so that the reaction mixture was only
147 in contact with the PET film and the 500 μm spacer. The reaction mixtures were injected into
148 the reaction cavity and the entire mould was placed in a UV chamber (model CL-1000
149 ultraviolet cross-linker, λ = 254 nm, output energy = 200 mJ/cm^2). The mould was turned
150 over every 5 mins for ca. 30 mins to promote an even cure on both surfaces of the mould.

151 **Table 1.**

152 Sample description, notation, type, composition and clay content.

Sample Description	Sample notation in figures	Sample type	tBA / mass%	PEGDMA / mass%	BTBD / mass%
tBA100/PEGDMA0	t100/P0	Film	100	0	0
tBA90/PEGDMA10	t90/P10	Film	90	10	0
tBA80/PEGDMA20	t80/P20	Film	80	20	0
tBA70/PEGDMA30	t70/P30	Film	70	30	0
tBA60/PEGDMA40	t60/P40	Film	60	40	0
tBA15/PEGDMA85	t15/P85	Film	15	85	0
tBA0/PEGDMA100	t0/P100	Film	0	100	0
tBA90/PEGDMA10/BTBD 0	t90/P10/BTBD 0	Film	90	10	0
tBA90/PEGDMA10/BTBD 1	t90/P10/BTBD 1	Film	90	10	1
tBA90/PEGDMA10/BTBD 3	t90/P10/BTBD 3	Film	90	10	3
tBA90/PEGDMA10/BTBD 5	t90/P10/BTBD 5	Film	90	10	5
tBA90/PEGDMA10/BTBD 0	t90/P10/BTBD 0 P	Coated on PET	90	10	0
tBA90/PEGDMA10/BTBD 1	t90/P10/BTBD 1 P	Coated on PET	90	10	1

153

154 In order to polymerise the tBA90/PEG10 mixture, with and without BTBD, onto the PET
155 film it was applied using a meter bar, producing a ca. 30 μm thick film. The coated film was
156 placed into a nitrogen gas filled chamber, equipped with a UV transparent window, and the
157 entire configuration was placed into the UV chamber for ca. 30 min.

158 *2.4 Characterisation Methods*

159 Swelling tests and ATR-FTIR Spectroscopy were used to confirm that cross-linking had
160 taken place and DSC traces (not illustrated) confirmed that the systems were fully cured**.**
161 Samples (10 mm^2) of tBA-*co*-PEGDMA network sheets were cut and weighed for their initial
162 mass, m_i, and separated into vials where they were immersed in 20 ml of propan-2-ol. The
163 samples were removed from the solvent periodically, dried lightly and weighed until an
164 equilibrium, swollen, mass, m_s, was reached. The equilibrium swelling ratio, q, was
165 calculated using the relationship, $q = m_s/m_i$.

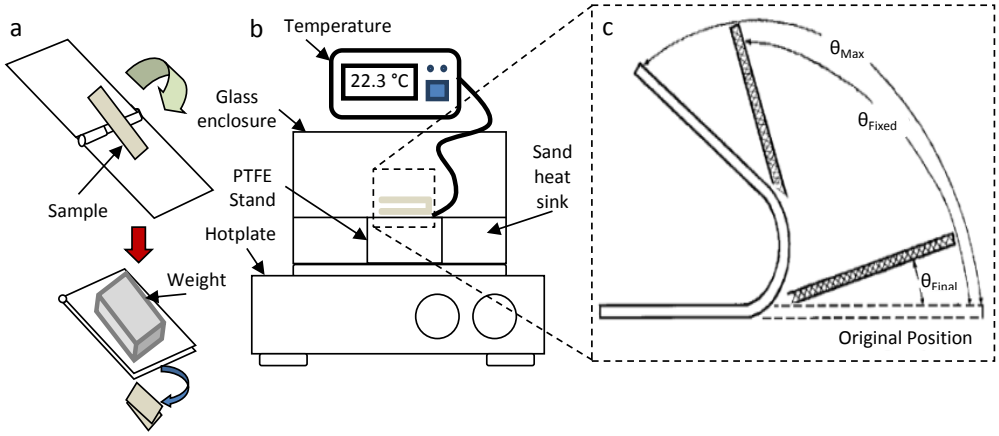

166

167 **Fig. 2.** Schematic illustration of a) the deformation method, b) the customised shape memory
168 effect (SME) evaluation platform and c) the shape recovery process. 1) Sample was heated
169 and deformed to a temporary shape using an external force, which applied a fixed
170 compression stress. 2) The sample was fixed into its temporary shape by rapid cooling in a
171 fridge, at 3±2°C, while the external force was maintained, θ_{Max}. 3) The external force was
172 removed and θ_{Fixed} °, was assessed. 4) The sample was placed in the heated chamber at a fixed
173 temperature and recovery to θ_{Final} was recorded over time (Lin and Wu, 1992).

174

175 The ATR-FTIR spectra were collected using a Nicolet, Nexus FT-IR model at room
176 temperature. X-ray diffraction traces of cast films were recorded, over an angular range of 5
177 to 40 °2θ, using a Philips X'Pert XRD, with a Cu X-ray source (λ = 1.542 Å), and a Philips
178 Miniprop detector. Dynamic Mechanical Analysis (DMA) was used to determine the

viscoelastic properties of the samples. A PerkinElmer model DMA8000 was employed in tension mode, with no pre-load, over a temperature range of -50 to 150°C, at a frequency of 1 Hz. The polymer samples, 25 x 5 (± 0.1) x 0.5 mm^3, were equilibrated at -50°C for 3 mins then raised to 90°C at a ramp rate of 3°C min^{-1}. The T_g was defined as the peak maximum of the tan δ curve. The rubbery modulus was determined from the storage modulus, when it had reached a steady state above the T_g as indicated by the unchanging tan δ curve.

The unconstrained shape memory capability of the tBA-*co*-PEGDMA and tBA90/PEGDMA10 BTBD networks was evaluated using a customised platform consisting of a hotplate, a glass enclosure and a temperature probe (Fig. 2). The hotplate was pre-heated to a temperature that was 10°C above the highest T_g of the samples under study, i.e. T_{high} = (T_g +10°C). The sample, 40 x 20 x 0.5 mm^3, was placed inside the enclosure for 10 mins to equilibrate at the T_{high} temperature. The sample was deformed, θ_{Max}, using a 250 g preheated steel weight and maintained at T_{high} in the enclosure, for an additional 5 mins while the sample was under strain, i.e. a fixed compression stress. The sample and the weight were taken from the enclosure and cooled to 3±2°C, T_{low}, in a fridge. At T_{low} the external force was removed and the fixed deformability, θ_{Fixed} °, was recorded. The sample was placed inside the heated glass enclosure, still at T_{high}, and the recovery angles, $\theta_i(t)$, that occurred during the shape memory evaluation were determined from still photographs captured, at appropriate time intervals, from video recordings. Once the sample had completed its transformation towards its permanent shape the value of θ_{Final} was recorded. Three replicate assessments of each sample were collected and the reproducibility was such that the data point size (in ~~Figures~~Figs. 6, 9 and 10) covers the sample to sample variation.

The unconstrained shape memory effect of uncoated PET and the coated PET samples, 60 x 20 x 0.03 mm^3, was determined by cutting slits in the flat samples (Fig. 3a) and placing them in the heated enclosure for 10 mins to equilibrate at the deformation temperature. They were

then deformed by inserting a cylindrical steel rod between the alternate strips of coated, or uncoated, PET (Fig. 3b). The deformed sample was then cooled in a fridge before the steel rod was removed and the sample placed in the chamber at T_{high}. The initial parameters noted were θ_{max} and θ_{Fixed}. A θ_{max} value of 100% reflected the ability of the sample to completely adopt the temporary shape under the influence of the deformation stress. If the sample relaxed after the stress was removed then this was recorded as θ_{Fixed}. Once these two initial parameters had been recorded a standard unconstrained shape memory evaluation was carried out with $\theta_i(t)$ being recorded photographically, as described above, every 30 ~~seconds~~s. When the sample transformation was complete, or the original shape recovered, θ_{Final} was recorded. The parameters extracted from the $\theta_i(t)$ versus time plot were $\theta_{1/2\ Final}$ Time, i.e. the time taken to recover 50% of the permanent shape, and θ_{Final} Time, the time taken to reach θ_{Final} i.e. the time taken to return to the permanent shape.

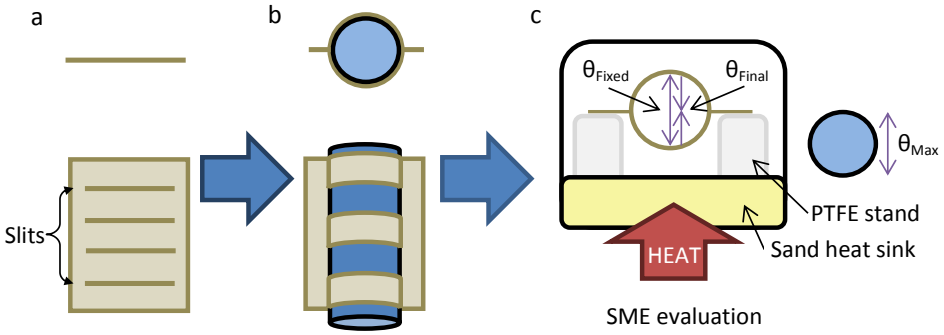

Fig. 3. Schematic illustration of the cylindrical deformation method for coated PET samples.

3. Results

3.1 Initial observations.

The complete absence of three diagnostic absorbance bands in the FTIR spectrum of tBA, assigned to C=C stretch (ca. 1636 and 1620 cm^{-1}) and the $C=CH_2$ twist (ca. 811 cm^{-1}) following photopolymerisation, together with the DSC data, confirmed that the reaction was

complete (Warren et al., 2010). As the cross link density increases a polymer becomes increasingly less able to swell and the level of equilibrium swelling, q, decreases (Ortega et al., 2008; Smith et al., 2009a~~10~~; Warren et al., 2010). Linear tBA, t100/P0, completely dissolved in propan-2-ol in a matter of hours indicating a complete absence of covalent cross-links. The equilibrium swelling ratios, q, for the networks, t90/P10 to t0/P100, in propan-2-ol decreased as the amount of PEGDMA, the cross-linking agent, increased (Fig. 4) confirming that the covalent cross-links acted to prevent polymer expansion and swelling.

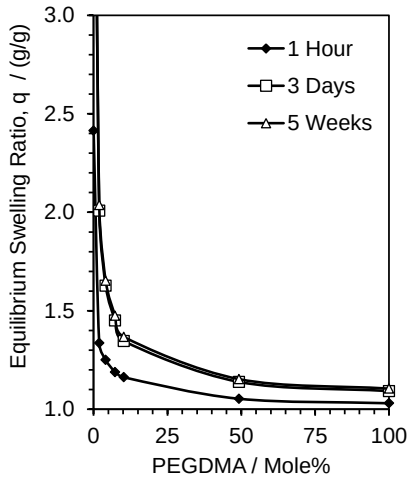

Fig. 4. Illustrative examples of the equilibrium swelling ratios, q, as a function of the mole percent of PEGDMA after 1 h, 3 days and 5 weeks immersion in propan-2-ol.

3.2 Shape memory behaviour of clay-free acrylate systems

3.2.1 Dynamic mechanical analysis

The temperature variation of the storage modulus and tan δ, of the t100/P0 to t0/P100 samples, were plotted as a function of temperature, -50 to 125°C (Fig. 5), and the relevant dynamic mechanical properties are summari~~s~~sed in Table 2.

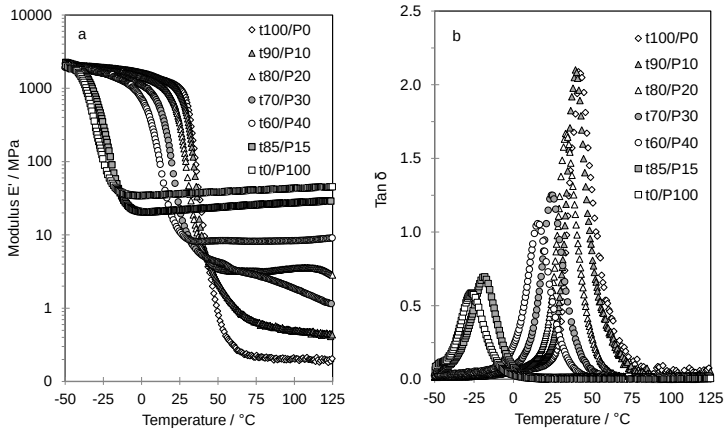

Fig. 5. Temperature dependence of a) storage modulus, and b) tan δ for the t100/P0 to t0/P100 networks over the temperature range -50 to 125°C.

Fig. 5a shows that the storage modulus at -50°C increased as the PEGDMA content increased (Table 2) as did the rubbery modulus (at ca. 100°C), whereas Fig. 5b shows that both the temperature at which the maximum in tan δ occurred, and the associated peak intensity, decreased with increased PEGDMA content. The temperature at which the modulus dropped sharply marked the onset of the $T_{g\alpha}$ transition, when large segments of the polymer chains gain sufficient thermal energy to begin moving, and established the starting point of the shape memory effect. Tsai et al., (2008) suggested that a sharp, at least one order of magnitude, decrease in storage modulus provides convincing evidence that a polymer system will demonstrate shape memory capability (Du and Zhang, 2010). The temperature at which the tan δ_{max} for a particular sample occurred (Fig. 5b) was used to define the T_g of the polymer system under investigation, while the intensity and shape of the tan δ peak provided information concerning the nature of the transformation from the temporary to the permanent shape. A sharp, intense tan δ_{max} peak followed by a reduction in tan δ to values below 0.5 indicates that a SMP will behave in a manner similar to an elastomer and display significant shape recovery when evaluated. In contrast, a low intensity tan δ_{max} indicates that a lesser shape recovery will occur (Chun et al., 2002, Tsai et al., 2008). Hence, a narrow, intense tan δ

peak indicates a fast transformation whereas a weak broad peak suggests that the transformation will be slower. A large, steep drop in storage modulus indicates that the energy stored in the deformation process will enable the SMP to exert a strong physical force as it returns to its permanent shape. This ability is particularly useful when the SMP has to work against an opposing force such as when used as a stent where it has to open up a collapsed blood vessel and keep it open (Ratna and Karger-Kocsis, 2008). Alternatively, when used as a suture it may be required to contract and in so doing pull two pieces of flesh together (Liu et al., 2009).

The initial storage modulus of the pure PEGDMA, t0/P100 (□, Fig. 5a), was 2129 MPa at -50°C and this steadily decreased reaching a value of 1903 MPa at -47°C. The T_g of this system was -26°C at which point the tan δ_{max} value was 0.6 tan δ (Fig. 5b). This latter value was sufficient to indicate that pure PEGDMA would exhibit shape memory capability, while the return to a tan δ of ca. 0 after the transition indicated that it should also behave like an elastomer. The reduction in modulus of the t0/P100 network was close to one and a half orders of magnitude, from 2129 MPa at -50°C to 34 MPa at the end of the $T_{g\alpha}$ transition. The gradual increase in the storage modulus to 42 MPa after the transition stage was attributed to thermally induced crystallisation (Smith et al., 2009a, b). Overall, pure PEGDMA (t0/P100) was predicted to exhibit some useful shape memory properties.

At -50 ˚C pure tBA, t100/P0, exhibited an initial storage modulus of ca. 2005 MPa (◊, Fig. 5a) which decreased steadily until ca. +22°C, when the modulus had reached ca. 1145 MPa. The narrow, high intensity tan δ_{max} value, of 2.1 tan δ, together with the return back to a tan δ value of zero (Fig. 5b), indicated that pure tBA would behave like an elastomer and display significant shape recovery when evaluated. At tan δ_{max} (41^{o}C) the modulus had reduced to ca. 22 MPa, and continued to decrease steadily until at the end of the $T_{g\alpha}$ transition it had reached

ca. 0.2 MPa. The drop in pure tBA storage modulus was almost four orders of magnitude; i.e. a very strong indication of a useful shape memory capability (Tsai et al., 2008).

Table 2.
Summary of the values obtained from dynamic mechanical analysis for the t100/P0 to t0/P100 networks over the temperature range -50 to 90°C.

Sample notation	Storage Modulus / MPa								$T_{g\alpha}$ / °C	Tan δ_{max}
	-50°C	-30°C	-10°C	10°C	30°C	50°C	70°C	90°C		
t100/P0	2005	1756	1605	1368	637	0.8	0.2	0.2	41	2.1
t90/P10	2108	1961	1782	1416	425	2	0.7	0.5	39	2.1
t80/P20	2035	1847	1597	1194	61	4	3	3	33	1.7
t70/P30	1923	1688	1342	659	10	4	3	2	24	1.3
t60/P40	2168	1719	1194	160	9	8	8	8	15	1.1
t15/P85	2249	759	27	21	22	24	25	27	-18	0.7
t0/P100	2129	292	36	35	37	39	41	42	-26	0.6

The systems with the more intense tan δ_{max} values, i.e. t90/P10 to t60/P40 (Table 2), were anticipated to exhibit significant shape recovery when evaluated whereas the lower tan δ_{max} value for the t15/P85 network (0.7 tan δ), offered a clear evidence that the shape recovery would be less dramatic (Chun et al., 2002, Tsai et al., 2008). Note that the 100-fold reduction in the storage modulus of the t90/P10 to t15/P15 networks provided good evidence for useful shape memory ability (Tsai et al., 2008, Du and Zhang, 2010). The increase in storage modulus as the PEGDMA content increased was anticipated as was the associated increase in the rubbery modulus (Kramer et al., 2010).

Overall the storage modulus, rubbery modulus and tan δ results, suggested that addition of PEGDMA to tBA resulted in a controllable shift, to lower temperatures, of the T_g and a reduction in the tan δ_{max} peak intensity. The rubbery storage modulus increased as the PEGDMA content increased in line with work with related systems (Gall et al., 2005; Ortega et al., 2008; Kramer et al., 2010).

3.2.2 Evaluation of the unconstrained shape memory effect

Unconstrained shape memory evaluation was employed to determine the extent to which each network would demonstrate shape memory and to explore the effect of increasing PEGDMA content on the speed and extent of shape reversal (Fig. 6). Cross-linked tBA-*co*-PEGDMA polymer networks are a class I type SMP, with a $T_{trans} = T_g$ (Liu et al., 2007). An appropriate SME temperature range to account for the different T_g values, which range from -26^{o}C for pure PEGDMA to +41^{o}C for pure tBA (Table 2), needed to be identified and a T_{high} value of 50°C, which was 10°C above the highest T_g, was chosen to ensure full shape recovery in all the relevant samples. Each network was annealed at 70°C for 15 mins prior to being deformed (Table 3).

Due to the higher PEGDMA, and hence cross-link, content the t60/P40 and t15/P85 networks were too brittle for an effective shape memory evaluation. The increased cross-link density most likely caused the stress-strain behaviour of the material to change from an elastomeric response to a stiff network with a pronounced brittle response (Ortega et al., 2008). The t100/P0 network exhibited a θ_{Max} of 100 % (Table 3), demonstrating that it was elastic enough to accommodate a high level of deformation stress. No recovery was observed after the deformation constraint was removed, thus a θ_{Fixed} value of 100 % was assigned, which demonstrated that the t100/P0 material could easily store the full amount of imparted strain. Yang et al. (2007) reported that at low temperatures, i.e. T_{low}, the entropy driven strain recovery forces are simply not sufficient to overcome the barrier to shape recovery. Consequently, the deformation cannot recover while the sample is maintained at T_{low}, even at long times, because the activation energy required to initiate recovery cannot be achieved.

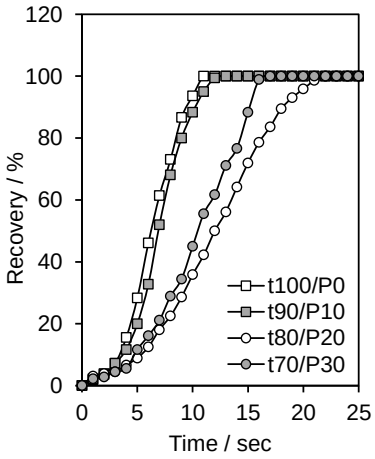

Fig. 6. Unconstrained recovery of the tBA-*co*-PEGDMA networks, from temporary shape to permanent shape, plotted against time at a fixed temperature, 50°C.

Shape memory recovery was carried out at 50°C and the recovery angle, $\theta_{i(t)}$, was recorded until the pure tBA reached a θ_{Final} of 100% (Fig. 6) which demonstrated that tBA was able to store the deformed strain at T_{low}, and return to its original shape. This agreed with literature predictions, (Ortega et al., 2008), in that low, possibly negligible, cross-link density should produce a SMP with a large recoverable strain but very little ability to generate force. The $\theta_{1/2\ Final}$ and θ_{Final} Times of recovery, ca. 6 and 11 ~~seconds~~s, respectively, demonstrated that the t100/P0 network recovered ca. 50 % of its permanent shape in ca. half of the time required to return to its permanent shape.

The t90/P10 to t70/P30 networks also displayed a θ_{Max} of 100 % indicating that although the PEGDMA content, and therefore the number of cross-links, had increased this did not increase ~~neither~~ the elasticity nor impair the ability to accommodate a high level of deformation strain ~~had been impaired~~. The θ_{Fixed} value was 100 % for all networks, t90/P10 to t70/P30, which indicated that increasing the PEGDMA content to 30 mass% did not diminish the network's ability to retain its temporary shape at T_{low}. The t90/P10 to t70/P30 networks demonstrated, by achieving a θ_{Final} of 100 %, that they were also capable of storing the deformed strain at T_{low} and could then return to their original shape. These networks also

behaved as anticipated, based on the DMA results (Fig. 6), which identified the propensity for large recoverable strains (Ortega et al., 2008). The $\theta_{1/2\ Final}$ and θ_{Final} Times of recovery (Table 3) demonstrated that the t90/P10 to t70/P30 networks also recovered 50 % of their permanent shape in ca. half the full recovery time.

Table 3.
Values, obtained using a T_{high} of 50°C, for the parameters θ_{Max}, θ_{Fixed}, $\theta_{1/2\ Final}$, θ_{Final}, $\theta_{1/2\ Final}$ Time, and θ_{Final} Time, which describe the recovery from temporary to permanent shape, for the samples described in Table 1.

Sample Description	Sample notation in figures	θ_{Max} / %	θ_{Fixed} / %	$\theta_{1/2\ Final}$ / %	θ_{Final} / %	$\theta_{1/2\ Final}$ Time / sec	θ_{Final} Time / sec
tBA100/PEGDMA0	t100/P0	100	100	50	100	6	11
tBA90/PEGDMA10	t90/P10	100	100	50	100	7	13
tBA80/PEGDMA20	t80/P20	100	100	50	100	12	22
tBA70/PEGDMA30	t70/P30	100	100	50	100	10	17
tBA90/PEGDMA10/BTBD 0	t90/P10/BTBD 0	100	100	50	100	7	12
tBA90/PEGDMA10/BTBD 1	t90/P10/BTBD 1	100	100	50	100	2.5	5.5
tBA90/PEGDMA10/BTBD 3	t90/P10/BTBD 3	100	100	50	100	4	9
tBA90/PEGDMA10/BTBD 5	t90/P10/BTBD 5	100	100	50	100	5	13
tBA90/PEGDMA10/BTBD 0 P	t90/P10/BTBD 0 P	100	93	41.5	90	52	540
tBA90/PEGDMA10/BTBD 1 P	t90/P10/BTBD 1 P	100	80	38.0	96	18	270

Overall these results indicated that as the PEGDMA content increased there was a corresponding increase in the $\theta_{1/2\ Final}$ and θ_{Final} Times of recovery. The t70/P30 network demonstrated faster $\theta_{1/2\ Final}$ and θ_{Final} Times of recovery than the t80/P20 network which may have its origins in that the increased number of cross-links could have enabled it to store larger amounts of energy culminating in a faster response. A complete assessment of the shape memory ability of the entire t100/P0 to t0/P100 system was not possible because of the brittleness of the t15/P85 and t0/P100 networks, but, it is almost certain that their shape recovery ability would be lower because highly cross-linked networks generally demonstrate low recoverable strain (Ortega et al., 2008). In effect these observations correspond well with

the DMA results which identified those networks with the ability to recover their permanent shape and exhibit large recoverable strains.

3.2.3 Summary of clay-free acrylate networks

The tBA-co-PEGDMA networks were fully cured and thermally stable, offering useful mechanical properties with most of the investigated combinations able to provide a shape memory response. Networks with high PEGDMA contents exhibited poor shape memory properties, being brittle and fracturing when subjected to large deformations. The t90/P10 network showed the most promise because it could be fully polymerised, offered useful mechanical properties, with similar elasticity and shape recovery capability to pure tBA, and had a rubbery modulus (above its T_g) capable of withstanding moderate mechanical load. However, even though this system returned to its permanent shape in only 13 ~~seconds~~s, it still exhibited relatively poor mechanical strength when compared to shape memory metal alloys (Lin and Wu~~et al.~~, 1992); a classic shortcoming of SMPs. The incorporation of well dispersed OC is known to enhance the mechanical properties of acrylate networks (Wu et al., 2010; Ingram et al., 2008; Oral et al., 2009) but the effect of clay incorporation on the shape memory properties has not previously been explored. Consequently, the consequences of adding BTBD to the t90/P10 system were investigated.

3.3 Shape memory behaviour of clay-acrylate nanocomposites

3.3.1 Initial observations

Swelling tests were carried out and ATR-FTIR spectra collected, as described in 3.2.1 above, which confirmed that the polymer networks had fully cured and formed cross-links and that all the BTBD-containing networks displayed similar swelling properties to the equivalent pure polymer (Fig. 4).

3.3.2 *X-ray diffraction data for shape memory nanocomposites.*

The XRD trace for BTBD powder (Fig. 7) displayed diffraction peaks at 4.2 °2θ (21.0 Å),19.7 °2θ (4.5 Å), and 35.0 °2θ (2.6 Å) which correspond to (001), (110,020) and (130, 200) reflections, respectively. The trace for the sample prepared without clay (t90/P10/BTBD 0) showed two broad reflections at 9.1 °2θ (9.7 Å) and 17.5 °2θ (5.1 Å) which were attributed to the polymer. The XRD traces for the systems containing 1, 3 and 5 mass% BTBD (t90/P10/BTBD 1, 3 and 5) all displayed a single peak at 4.5 °2θ (19.6 Å) as well as the two reflections associated with the polymer, at 9.5 °2θ (9.7 Å) and 17.5 °2θ (5.1 Å). The diffraction peaks associated with BTBD at 19.7 °2θ (4.5 Å) and 35.0 °2θ (2.6 Å) were too weak to be seen at these addition levels.

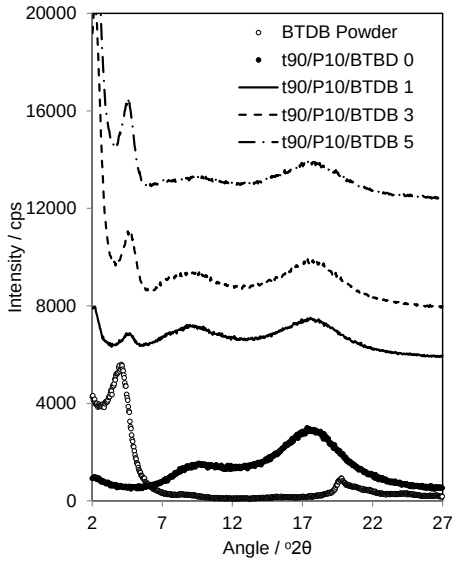

Fig. 7. Cu XRD traces of BTBD and the t90/P10/BTBD 0 to 5 networks.

The low angle reflection associated with BTBD, in the BTBD-containing networks, appeared at slightly higher angles than that of the BTBD powder (Fig. 7). Vaia and Liu (2002) have advised caution when tempted to overstate the consequences of small shifts in the positions of reflections in CPN, because several factors can contribute to a decrease in diffraction peak

intensity and uncertainty concerning the distance between the layers. The apparent reduction in basal spacing from 21.0 to 19.6 Å could indicate a reduction in the interlayer content but a more likely explanation, in accord with Vaia and Liu's interpretation, is that the shift arises from a change in the number of layers per stack and angular variations between layers in a stack. Nonetheless, the diffraction data confirmed that polymerisation did not occur, nor was polyacrylate present, in the interlayer space. The apparent absence of poly(tBA-*co*-PEGDMA) in the interlayer contrasts with the report of Ingram et al., (2008) who found that quaternary (bis-2-hydroxyethyl) methyl tallowammonium-exchanged Cloisite, C30B, formed exfoliated/intercalated CPN in a radically-initiated methylmethacrylate (MMA) network. The XRD trace for MMA containing 1 and 2 mass% C30B exhibited no diffraction peaks leading the authors to suggest full exfoliation, whereas the XRD trace for the 4 mass% 30B/MMA sample displayed a reflection at 2.1 °2θ (42.0 Å) indicating that an intercalated CPN had been produced.

3.3.~~2~~3 Dynamic mechanical analysis of clay-acrylate nanocomposites

The storage modulus and tan δ values, for the t90/P10/BTBD 0 to 5 networks, are plotted in Fig. 8 over the temperature range, -50 to +125°C, and the associated values for the properties of interest are summari~~s~~z~~z~~ed in Table 4. The data for the t90/P10/BTBD 0 sample was described above (t90/P10, Fig. 5, Table 2) and the samples prepared by incorporation of BTDB into this host matrix, t90/P10/BTBD 1 to 5, exhibited initial storage moduli of ca. 1949, 1629 and 1702 MPa, respectively, at -50°C which steadily decreased reaching values of ca. 1417, 1040 and 1083 MPa at 12°C. The ensuing steep drop in the moduli established the starting point of the shape memory effect and resulted in reductions of at least three and a half orders of magnitude in modulus, reaching 1.0, 0.5 and 0.6 MPa, respectively, at 150^{o}C.

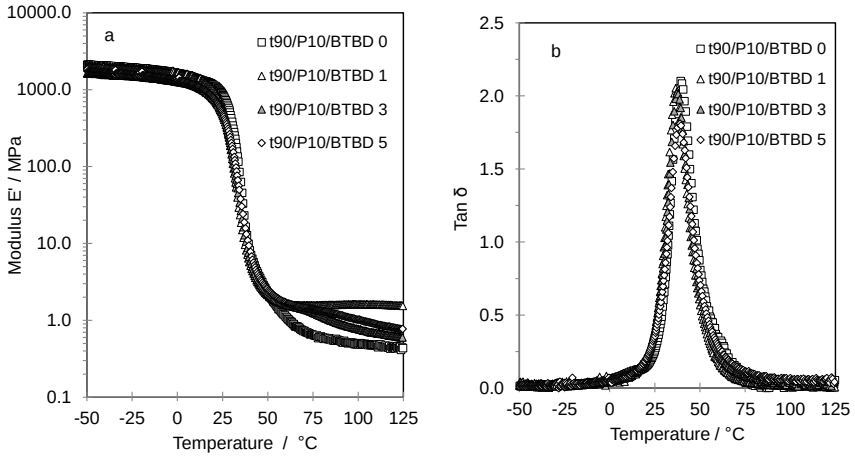

Fig. 8. Temperature dependence of a) storage modulus, b) tan δ of the t90/P10/BTBD 0 to 5 networks over the temperature range -50 to 125°C.

The T_g values for the t90/P10/BTBD 1, 3 and 5 samples were very similar at 37, 37 and 38°C, respectively. The corresponding tan δ_{max} values, 2.1, 2.0 and 1.8 tan δ, taken together with the reduction in the associated tan δ values to zero, were large enough to confidently predict that these networks would display elastomeric behaviour and exhibit useful shape memory properties. However, these results were remarkably similar to the t90/P10 host polymer so no dramatic increase in shape memory capability was expected.

Table 4.
Summary of the values obtained from dynamic mechanical analysis for the t90/P10/BTBD 0 to 5 networks over the temperature range -50 to 150°C.

Sample Description	Storage Modulus / MPa							T_g / °C	Tan δ_{max}
	-50°C	-25°C	0°C	25°C	50°C	100°C	150°C		
t90/P10/BTBD 0	2108	1928	1629	876	2	0.5	0.4	40	2.1
t90/P10/BTBD 1	1949	1808	1563	549	2	2.0	1.0	37	2.1
t90/P10/BTBD 3	1629	1562	1276	459	2	0.8	0.5	37	2.0
t90/P10/BTBD 5	1702	1564	1322	508	3	1.0	0.6	38	1.8

The DMA results confirmed that the incorporation of BTBD resulted in no significant shift of the T_g and only small reductions in the tan δ_{max} peak intensity; as noted for shape memory

clay-epoxy nanocomposites (Liu et al., 2011). The rubbery modulus of the t90/P10/BTBD 1 network was more than twice that of the other, clay-containing, networks indicating that it could maintain greater mechanical loading than the other systems when $T > T_g$. Benfarhi et al. (2004) and Okamoto et al. (2000) also noted that the highest modulus was obtained with a clay loading of ca. 1 mass% in related, non-SMP, acrylate CPN. However, as the BTBD content was increased the initial storage modulus decreased from that of the host matrix which corresponded to reports where acrylate networks, PU-based acrylates and epoxy-based acrylates, exhibited a drop in initial storage modulus with increasing clay content (Benfarhi et al., 2004; Keller et al., 2004). It is, however, more common for the initial storage modulus to increase when the OC is effectively dispersed throughout the polymer matrix(Okamoto et al., 2001; Shemper et al., 2004; Decker et al., 2005; Xu et al., 2006; Zang et al., 2009).

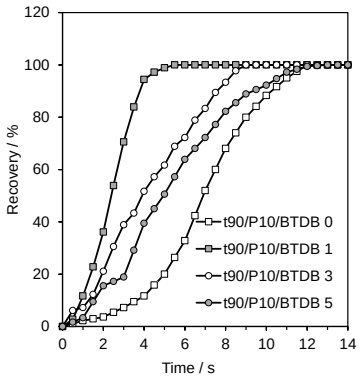

Fig. 9. Unconstrained SME testing of t90/P10/BTDB 0 to 5 networks, from temporary to permanent shape, plotted against time at a fixed temperature, 50°C.

3.3.~~3~~4 *Evaluation of the unconstrained shape memory effect*

The unconstrained shape memory ability was evaluated to establish whether the BTBD-containing networks would demonstrate shape memory and to determine the effect of BTBD content (Fig. 9). The close proximity of the T_g values for the different samples meant that a single deformation regime was appropriate. Table 3 summarises the properties of interest.

Once again the values of θ_{Final}, $\theta_{1/2\ Final}$ Time and θ_{Final} Time (Fig. 9, Table 3) confirmed that the clay-free network stored the full load of imposed strain and that it recovered 50% of its permanent shape in half the time required for full recovery. The t90/P10/BTBD networks also displayed a θ_{Max} of 100 %, confirming that the BTBD content did not retard the elasticity nor reduce the networks' ability to accommodate a high level of deformation strain. The θ_{Fixed} results were also 100 % for all these systems confirming that an increased BTBD content did not diminish the ability of the networks to retain their temporary shape. Reaching a θ_{Final} of 100 % proved that these networks could store the deformed strain and return to their permanent shape. The $\theta_{1/2\ Final}$ and θ_{Final} Times of recovery (Table 3) demonstrated that the BTBD-containing samples also recovered 50 % of their permanent shape in ca. half the full recovery time. Most of these observations corresponded well with the results predicted by DMA, but the DMA data was singularly unable to predict the extent to which the presence of BTBD accelerated the rate of permanent shape recovery. The fastest return to the permanent shape was achieved when 1 mass% BTBD was incorporated. Liu et al. (2011) also observed that the θ_{Final} Times of recovery for clay-epoxy ~~SMP~~SMPs did not vary systematically with OC content and the shortest recovery time occurred when 3 mass% of a cetyltrimethylammonium-clay was used. The authors attributed this non-systematic variation to a reduction in OC dispersion at loadings of 4 and 5 mass%.

3.3.~~4~~5 Imparting shape memory effect to PET film

The t90/P10/BTBD 1 network demonstrated the fastest return to its permanent shape and exhibited the largest rubbery modulus (2.0 MPa) so it was chosen as the preferred system to coat onto a PET substrate. The aim was to determine whether this acrylate network could confer shape memory capability to the PET substrate and whether the presence of BTBD offered any additional capability (Fig. 10). The t90/P10/BTBD 0 and 1 coated PET substrate

and uncoated PET sheet were deformed, after annealing at 70°C, and their shape memory recoveries determined as described in Ssection 2.4 (Fig. 2 and 3).

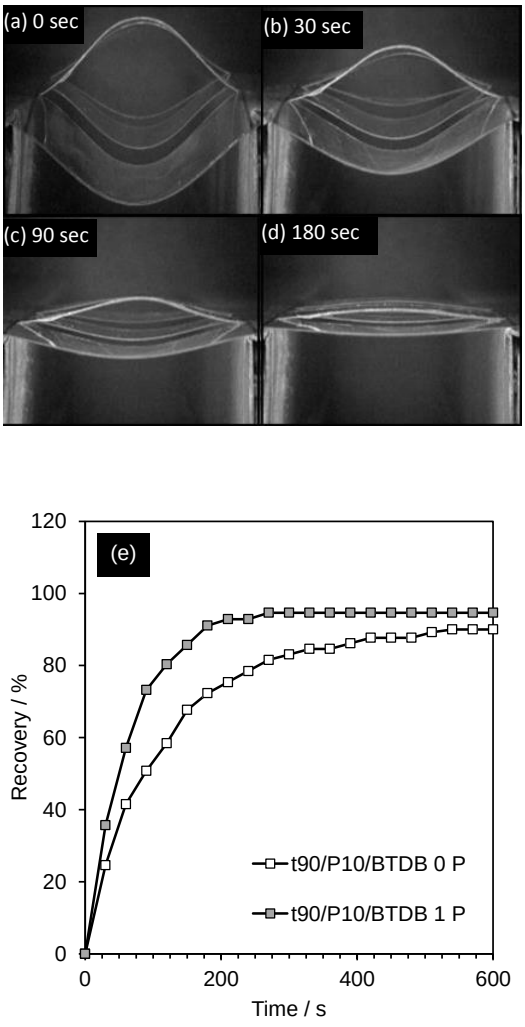

Fig. 10. Unconstrained SME testing of t90/P10/BTBD 0 and 1 coated PET substrates, from temporary to permanent shape. Video capture images of a t90/P10/BTBD 1 SMP coated PET at sequential time intervals (a) 0, (b) 30, (c) 90 and (d) 180 sec; (e) recovery % against time. All data were obtained at a fixed temperature, 50°C.

The uncoated PET sample was deformed to a θ_{Max} of 100 % (Fig. 3) and cooled to T_{low}, 0 to 5°C. Upon removal of the steel rod the uncoated PET sample immediately collapsed;

dramatically demonstrating a θ_{Fixed} value of 0 %. The t90/P10/BTBD 0 coated substrate was deformed in the same manner and achieved a θ_{Max} of 100 % demonstrating that the shape memory coating had accommodated the deformation stress but the sample relaxed a little at T_{low} leading to a θ_{Fixed} value of 93 %. This confirmed that the t90/P10/BTBD 0 P coated substrate could be deformed to a large degree and was able to store the majority of the imposed strain, in marked contrast to the behaviour of the uncoated PET which collapsed back to its permanent (flat) shape when the steel rod was removed. The t90/P10/BTBD 0 P sample reached an ultimate recovery, θ_{Final}, of 90 % with corresponding $\theta_{1/2\ Final}$ and θ_{Final} Times of 90 and 540 ~~seconds~~s, respectively, showing that the t90/P10/BTBD 0 P coated substrate recovered 50 % of the θ_{Final} very rapidly compared to the full recovery time.

The t90/P10/BTBD 1 P coated substrate exhibited a θ_{Max} of 100 % and a θ_{Fixed} of 80 % proving that it was also able to accommodate, and store, a high level of deformation stress, albeit less than the pure acrylate coated substrate. The t90/P10/BTBD 1 coated PET substrate achieved a θ_{Final} of 96 % which demonstrated that neither the t90/P10/BTBD 0 nor t90/P10/BTBD 1 coated PET were able to fully return to their permanent, flat shape. The $\theta_{1/2Final}$ and θ_{Final} Times of recovery for the t90/P10/BTBD 1 P sample were 18 and 270 ~~seconds~~s, respectively, which demonstrated that the presence of as little as 1 mass% BTBD in a shape memory CPN could significantly accelerate the rate of permanent shape recovery of a coated substrate.

4. Conclusions

The tBA-*co*-PEGDMA crosslinked networks displayed useful shape memory properties up to PEGDMA contents of 40 %. Above this PEGDMA content the materials were prone to fracture and too brittle for a realistic assessment of their shape memory capability. The tBA90/PEGDMA10 material was selected as the host matrix to investigate the effect of

incorporating OC on the shape memory capability. X-ray diffraction data confirmed that BTBD formed a microcomposite in the selected matrix and hence exerted no influence on the storage modulus, rubbery modulus, glass transition temperature, T_g, or the shape or intensity of the tan δ peak of the host matrix. Therefore, it was anticipated that the presence of BTBD would have no effect, positive or negative, on the shape memory properties of the host matrix. However, it was found that the incorporation of clay, especially at the 1 mass% level, significantly accelerated the speed at which the microcomposite returned to the original, permanent shape. This accelerated return to the permanent shape, compared to the clay-free SMP, was also observed when the microcomposite was coated onto a 100 μm PET film.

5. Acknowledgements

MB gratefully acknowledges support from the Engineering and Physical Science Research Council via a CASE Award (Voucher Number 08002513).

References

Annabi-Bergaya F., 2008. Layered clay minerals. Basic research and innovative composite applications. Microporous and Mesoporous Mater. 107, 141-148.

Behl M., Razzaq M.Y., Lendlein A., 2010. Multifunctional Shape-Memory Polymers. Adv. Mater. 22, 3388-3410.

Benfarhi S., Decker C., Keller L., Zahouily K., 2004. Synthesis of clay nanocomposite materials by light-induced crosslinking polymerization. Eur. Polym. J. 40, 493-501.

Cao F., Jana S.C., 2007. Nanoclay-tethered shape memory polyurethane nanocomposites. Polymer. 48, 3790-3800.

Chun B.C., Cha S.H., Chung Y.C., Cho J.W., 2002. Enhanced dynamic mechanical and shape-memory properties of a poly(ethylene terephthalate)-poly(ethylene glycol) copolymer crosslinked by maleic anhydride. J. Appl. Polym. Sci. 83, 27-37.

Chung Y-C., Choi J.W., Park J.S., Shin C.H., Chun B.C., 2011. Covalent bonding of surface-modified montmorillonite nanoparticle with polyurethane and its impact on shape memory effect and mechanical properties. J. Thermoplatic Composite Materials. 24, 477-497.

Decker C., Keller L., Zahouily K., Benfarhi S., 2005. Synthesis of nanocomposite polymers by UV-radiation curing. Polymer. 46, 6640-6648.

Du H.Y., Zhang J.H., 2010. Shape memory polymer based on chemically cross-linked poly(vinyl alcohol) containing a small number of water molecules. Colloid. Polym. Sci. 288, 15-24.

Gall K., Yakacki C.M., Liu Y.P., Shandas R., Willett N., Anseth K.S., 2005. Thermomechanics of the shape memory effect in polymers for biomedical applications. J. Biomed. Mater. Res. A, 73A, 339-348.

Ge Q., Luo X.F., Iversen C.B., Mather P.T., Dunn M.L., Qi H.J., 2013. Mechanisms of triple-shape polymeric composites due to dual thermal transitions. Soft Matter. 9, 2212–2223.

Haghayegh M., Sadeghi G.M.M., 2012. Synthesis of shape memory polyurethane/clay nanocomposites and analysis of shape memory, thermal and mechanical properties. Polym. Comp. 843-849.

Ikematu T., Kishimoto Y., and Miyamoto K., 1993. Shape memory polymer resin composition and the shape memorizing moulded product thereof. Japan Patent 5189110.

Ingram S., Dennis H., Hunter I., Liggat J.J., McAdam C., Pethrick R.A., Schaschke C., Thomson D., 2008. Influence of clay type on exfoliation, cure and physical properties of in situ polymerised poly(methyl methacrylate) nanocomposites. Polym. Int. 57, 1118-1127.

Jiang H.Y., Kelch S., and Lendlein A., 2006. Polymers move in response to light. Adv. Mater. 18, 1471-1475.

Keller L., Decker C., Zahouily K., Benfarhi S., Le Meins J.M., Miehe-Brendle J., 2004. Synthesis of polymer nanocomposites by UV-curing of organoclay-acrylic resins. Polymer. 45, 7437-7447.

Kramer N.J., Sachteleben E., Ozaydin-Ince G., van de Sanden R., Gleason K.K., 2010. Shape memory polymer thin films deposited by initiated chemical vapor deposition. Macromolecules. 43, 8344-8347.

Formatted: Spanish (Spain-Traditional Sort)

Formatted: English (U.K.)

Formatted: English (U.K.)

584 Lendlein A., Kelch S., 2002. Shape-memory polymers. Angew. Chem. Int. Edn. 41, 2035-
585 2057.
586 Lendlein A., Langer R., 2002. Biodegradable, elastic shape-memory polymers for potential
587 biomedical applications. Science. 296, 1673–1676
588 Liff S.M., Kumar N., McKinley G.H., 2007. High-performance elastomeric nanocomposites
589 via solvent-exchange processing. Nat. Mater. 6, 76-83.
590 Lin H.C., Wu S.K., 1992. Strengthening effect on shape recovery characteristic of the
591 equiatomic TiNi alloy .Scripta Metall., 26, 59–62
592 Liu C., Qin H., Mather P.T., 2007. Review of progress in shape-memory polymers. J.Mater.
593 Chem. 17, 1543-1558.
594 Liu Y., Han C., Tan H., Du X., 2011. Organic-montmorillonite modified shape memory
595 epoxy resin. 22, 2017-2021.
596 Liu Y.J., Lu H.B., Lan X., Leng J.S., Du S.Y., 2009. Review of electro-activate shape-
597 memory polymer composite. Compos. Sci. Technol. 69, 2064–2068
598 Maitland D. J., Metzger M. F., Schumann D., Lee A., 2002. Photothermal properties of shape
599 memory polymer micro-actuators for treating stroke. Laser. Surg. Med. 30, 1-11.
600 Migneco F., Huang, Y.C., Birla R.K., Hollister S.J., 2009. Poly(glycerol-dodecanoate), a
601 biodegradable polyester for medical devices and tissue engineering scaffolds.
602 Biomaterials, 30, 6479-6484.
603 Okamoto M., Morita S., Kim Y.H., Kotaka T., Tateyama H., 2001. Dispersed structure
604 change of smectic clay/poly(methyl methacrylate) nanocomposites by copolymerization
605 with polar comonomers. Polymer. 42, 1201-1206.
606 Okamoto M., Morita S., Taguchi H., Kim Y.H., Kotaka T., Tateyama H., 2000. Synthesis and
607 structure of smectic clay/poly(methyl methacrylate) and clay/polystyrene
608 nanocomposites via in situ intercalative polymerization. Polymer. 41, 3887-3890.
609 Oral A., Tasdelen M.A., Demirel A.L., Yagci Y., 2009. Poly(methyl methacrylate)/clay
610 nanocomposites by photoinitiated free radical polymerization using intercalated
611 monomer. Polymer. 50, 3905-3910.
612 Ortega A.M., Kasprzak S.E., Yakacki C.M., Diani J., Greenberg A.R., Gall K., 2008.
613 Structure-property relationships in photopolymerizable polymer networks: Effect of
614 composition on the crosslinked structure and resulting thermomechanical properties of a
615 (meth)acrylate-based system. J. Appl. Polym. Sci. 110, 1559-1572.
616 Quadrini F., Santo L., Squeo E.A., 2012. Solid-state foaming of nano-clay-filled thermoset
617 foams with shape memory properties. Polymer-Plastics Technology and Engineering 51,
618 560-567.
619 Ratna D., Karger-Kocsis J., 2008. Recent advances in shape memory polymersa nd
620 composites: a review. J. Mater. Sci. 43, 254-269.
621 Rezanejad R., Kokabi M., 2007. Shape memory and mechanical properties of cross-linked
622 polyethylene/clay nanocomposites. Eur. Polym. J. 43, 2856 -2865
623 Safranski D.L., Gall K., 2008. Effect of chemical structure and crosslinking density on the
624 thermo-mechanical properties and toughness of (meth)acrylate shape memory polymer
625 networks. Polymer. 49, 4446-4455.

Formatted: English (U.K.)

Formatted: English (U.K.)

Formatted: Spanish (Spain-Traditional Sort)

Formatted: English (U.K.)

626 Shemper B.S., Morizur J.F., Alirol M., Domenech A., Hulin V., Mathias L.J., 2004. Synthetic
627 clay nanocomposite-based coatings prepared by UV-cure photopolymerization. J. Appl.
628 Polym. Sci. 93, 1252-1263.
629 Smith K.E., Parks S.S., Hyjek M.A., Downey S.E., Gall K., 2009a The effect of the glass
630 transition temperature on the toughness of photopolymerizable (meth)acrylate networks
631 under physiological conditions. Polymer. 50, 5112-5123.
632 Smith K.E., Temenoff J.S., Gall K., 2009b. On the toughness of photopolymerizable
633 (meth)acrylate networks for biomedical applications. J. Appl. Polym. Sci. 114, 2711-
634 2722.
635 Tao X., 2010. Tunable polymer multi-shape memory effect. Nature. 464, 267-270
636 Tong T.H., 2004. Shape memory styrene copolymer. Patent US6759481 B2.
637 Tsai Y., Tai C.H., Tsai S.J., Tsai F.J., 2008. Shape memory effects of poly(ethylene
638 terephthalate-co-ethylene succinate) random copolymers. Eur. Polym. J. 44 , 550-554.
639 Utracki L.A., 2010. Clay-Containing Polymeric Nanocomposites and Their Properties. IEEE
640 Electr. Insul. M. 26, 6-15
641 Vaia R.A., Liu W.J., 2002. X-ray Powder Diffraction of Polymer/Layered Silicate
642 Nanocomposites: Model and Practice. J. Polym. Sci. Polym. Phys. 40, 1590-1600.
643 Venkatraman S.S., Tan L.P., Joso J.F., Boey Y.C., Wang X., 2006. Biodegradable stents with
644 elastic memory. Biomaterials. 27, 1573–1578
645 Voit W., Ware T., Dasari R.R., Smith P., Danz L., Simon D., Barlow S., Marder S.R., Gall
646 K., 2010. High-strain shape-memory polymers. Adv. Funct. Mater. 20, 162-171.
647 Warren P.D., McGrath D.V., and Geest J.P.V., 2010. Effect of crosslinker length and
648 composition on the hydrophobicity and thermomechanical response of acrylate-based
649 shape-memory polymers. Macromol. Mater. Eng. 295, 386-396.
650 Wu G.L., Liu G.P., Zang Y.L., Lu Y.B., Xiong Y.Q., Xu W.J., 2010. Preparation and
651 characteration of UV-cured EA/MMT nanocomposites via in-situ polymerization. J.
652 Macromol. Sci. A. Pure. Appl. Chem. 47, 647-654.
653 Wu T., O'Kelly K., Chen B., 2013. Poly(methylmethacrylate)-grafted clay-thermoplastic
654 e;astomer composites with water - induced shape-memory effects. J. Polym. Sci. Polym.
655 Phys. 51, 1513-1522.
656 Xu B., Huang W.M., Pei Y.T., Chen Z.G., Kraft A., Reuben R., De Hossen J.Th.M., Fu Y.Q.
657 2009. Mechanical properties of attapulgite clay reinforced polyurethane shape-memory
658 nanocomposites. 45, 1904-1911.
659 Xu Y.J., Brittain W.J., Vaia R.A., Price G., 2006. Improving the physical properties of
660 PEA/PMMA blends by the uniform dispersion of clay platelets. Polymer. 47, 4564-4570.
661 Yakacki C.M., Shandas R., Safranski D., Ortega A.M., Sassaman, K., Gall K., 2008. Strong,
662 tailored, biocompatible shape-memory polymer networks. Adv. Funct. Mater. 18, 2428-
663 2435
664 Yang F., Wornyo E., Gall K., King W.P., 2007. Nanoscale indent formation in shape memory
665 polymers using a heated probe tip. Nanotechnology. 18, 285302.
666 Zang Y.L., Xu W.J., Liu G.P., Qiu D.Y., Su S.P., 2009. Preparation of ultraviolet-cured
667 bisphenol A epoxy diacrylate/montmorillonite nanocomposites with a bifunctional,
668 reactive, organically modified montmorillonite as the only initiator via in situ. J. Appl.
669 Polym. Sci. 111, 813-818.